Novel Ionospheric Activity Indicator Specifically Tailored for GNSS Users

J. Sanz, J.M. Juan and G. González-Casado, *Research Group of Astronomy and Geomatics, Technical University of Catalonia, Spain, gAGE/UPC*
R. Prieto-Cerdeira, S. Schlüter and R. Orús, *European Space Agency, ESA*

BIOGRAPHY

Dr. J. Sanz Subirana is senior researcher at gAGE/UPC. His current research interests are in the area of GNSS data processing algorithms, GNSS ionospheric sounding, augmentation systems (SBAS and GBAS), and High Accuracy GNSS Navigation.

Dr. J.M. Juan Zornoza is senior researcher at gAGE/UPC. His current research interests are in the area of GNSS data processing Algorithms for High Accuracy GNSS Navigation and GNSS ionospheric sounding, as well as Augmentation Systems (SBAS and GBAS).

Dr. G. González-Casado is senior researcher at gAGE/UPC. His current research interests are GNSS data processing and ionospheric sounding, high accuracy GNSS Navigation and Augmentation Systems (SBAS and GBAS).

Mr. R. Prieto-Cerdeira is a GNSS R&D Engineer working for the GNSS Evolutions Programme and Strategy Division of the European Space Agency.

Dr. S. Schlüter is a research fellow at the DLR (German Aerospace Center) at the Institute of Communications and Navigation. In 2010 he joined the team of the ESA EGNOS Project Office in Toulouse as a seconded expert. At present he is responsible for the coordination of technical aspects related to EGNOS ionospheric processing and algorithm development.

Dr. R. Orús has a Physics degree from the University of Barcelona (UB) and a PhD in Aerospace Science and Technology from the gAGE/UPC research group of the Technical University of Catalonia (UPC). Since 2010, he joined the Electromagnetics and Space Environment Division of ESA/ESTEC as a Propagation Engineer working on activities related to radio-wave propagation in troposphere and ionosphere for GNSS and other ESA projects.

ABSTRACT

This work introduces a novel ionospheric activity indicator useful for identifying disturbed periods affecting performance for GNSS users, at regional level. This indicator is based in the "Along Arc TEC Rate (AATR) and can be easily computed from GNSS data.

The AATR indicator has been assessed over more than one Solar Cycle (2002-2013) involving 140 receivers distributed world-wide. Results show that it is well correlated with the ionospheric activity and, unlike other global indicators linked to the geomagnetic activity (i.e. *DST*, *Ap*), it is sensitive to regional behaviour the ionosphere and identifies specific effects on GNSS users. Moreover from a devoted analysis of EGNOS performances in different ionospheric conditions, it follows that the *AATR* indicator is able to predict SBAS user availability anomalies linked to the ionosphere.

The AATR indicator has been chosen as the metric to characterise the ionosphere operational conditions in the frame of EGNOS activities. This indicator has been also proposed for joint analysis in the International SBAS-Ionosphere Working Group.

INTRODUCTION

The ionosphere is a highly variable and hardly predictable environment. Phenomena of different geographical and temporal characteristics may affect the performance of ionospheric monitoring methods based on real-time GNSS measurement data. Due to the complexity of the phenomenology of the ionosphere, it has always been a challenge for satellite navigation engineers to find a simple metric to characterise the state of the ionosphere in a simple manner and at regional level. In particular, such a metric could serve the definition of technical specifications which would be related to availability and integrity performances, and could support the qualification process of the system. It would also allow the identification of disturbed periods in quasi-real-time.

Satellite Based Augmentation Systems (SBAS) provide differential corrections and confidence bounds to guarantee user navigation with improved accuracy and compliance with high integrity requirements. One of these corrections is the ionospheric delay, which is the error component most difficult to model.

In general, the ionospheric corrections are computed from linear models fed by GNSS measurements collected from permanent receiver's networks, where the ionospheric delays or Slant Total Electron Content (STEC) seen by the reference stations are, in some way, linearly interpolated to the user position. But under increased ionospheric activity, the linearity assumption in the STECs behaviour is far from being fulfilled, potentially leading to significant errors. In this sense, the performance of the ionospheric model (relaying on linear fits) is linked to the ionospheric activity, which can depend on many factors such as year, season, local time, geographical location or geomagnetic activity.

Taking into account the previous considerations, it is then necessary to identify and to study the ionospheric disturbed periods in order to protect the users against ionospheric threats.

Several attempts have been done in order to characterise the ionospheric activity over wider regions with a single parameter. For instance, in [1] and [2] the Disturbed Storm Time *(DST*) index is used for identifying such periods. In these works a correlation better than 0.5 is found between the *DST* and an indicator of the lack o linearity of the ionospheric model (adjusted with data gathered by North American receivers during geomagnetic storms).

But there are evidences that ionospheric activity depends on other factors that cannot be linked to a global index. In this sense, an index associated to the STECs measurements from a specific receiver was defined in [3] and [4], which allowed to take into account some local/regional characteristics of the ionospheric activity.

The approach for the European SBAS, EGNOS, foresees the following scheme [5]: first the specification of ionospheric conditions using the ionospheric indicator presented in this paper, and, based on these specification, the generation of realistic ionospheric reference scenarios in order to support algorithm development and qualification. These scenarios, generated from real data shall be representative of both quiet and disturbed ionospheric conditions over sufficiently long periods.

In this work, we define a new ionospheric activity indicator which enables to detect regional ionospheric disturbances and can be easily computed from the GNSS data. For a given receiver, this indicator is based on the hourly weighted root-mean-square (RMS) of the AATR.

THE AATR INDEX

For a given transmitter-receiver pair, the variation over time of the STEC (Along Arc STEC Rate, $AASR_i$) can be computed as:

$$AASR_i = \frac{\Delta STEC_i}{\Delta T} \tag{1}$$

where i indicates the observation epoch, $\Delta STEC_i$ corresponds to the difference of STECs between two consecutive observations in the same satellite-receiver arc and ΔT is the elapsed time between these consecutive observations (typically 30 or 60 seconds).

The vertical TEC rate can be obtained by divining the previous expression by the mapping function or obliquity factor $M(\varepsilon)$. In our case, we apply this mapping squared in order to mitigate the effect of low elevation rays (instead of applying a cut-off angle). Then

$$AATR_i = \frac{1}{M(\varepsilon)}\frac{AASR_i}{M(\varepsilon)} = \frac{\Delta STEC_i}{\left(M(\varepsilon)\right)^2 \Delta T} \tag{2}$$

From previous equation (2), we define the ***AATR indicator*** as the **hourly weighted RMS of the $AATR_i$ instantaneous values** computed from the measurements collected by a given receiver,

$$AATR = \sqrt{\frac{1}{N}\sum_{i=1}^{N} AATR_i^2} \tag{3}$$

where N is the number of observations in 1 hour.

Notice that, as other ionospheric activity indicators (e.g. the rate of change of TEC [8] or rate of TEC gradient [3]), the AATR defined above uses the variation over time of the STEC for a specific transmitter-receiver pair ($AASR_i$), as basic measurement. But, unlike these other indicators (basically thought for detecting small irregularities like scintillation), the AATR takes also into account the dispersion of the $AATR_i$ values of all the measurements from a specific receiver.

Moreover, as it is known, *AASR* can be expressed as:

$$AASR_i = \frac{\Delta STEC_i}{\Delta T} \simeq \frac{\partial STEC_i}{\partial T} + \nabla STEC_i \cdot \mathbf{v}_{i\,pp} \tag{4}$$

where $\mathbf{v}_{pp}$ is the velocity of the ionospheric pierce point and $\nabla STEC$ is the spatial gradient of the STEC. Thus, the AATR is sensitive to spatial gradients, temporal variations of STEC (for instance a Solar Flare) and, because it is a RMS, it is also sensitive to the dispersion of the STEC rates (as occurs under scintillation and ionospheric storms).

Performance of the AATR index during high ionospheric activity

As commented above, large gradients or other ionospheric anomalies lead to a lack of linearity, degrading the performance of the linear models used to compute the ionospheric corrections. The ionospheric activity can be identified from the mis-modelling of such linear models, by analysing the signatures of the post-fit residuals. An example is shown in Figure 1 where the RMS of the post-fit residuals from a two-layers accurate ionospheric model [6] is shown (in red) over a week around the Halloween storm (from days 298 to 305 of year 2003). The plot at top is for the station POTS in the North or Europe ($\phi \sim 55^{o}$) and the plot at the middle for the station LLIV in the south of Europe ($\phi \sim 41^{o}$).

The AATR indices of the two previous receivers and also of two other receivers (BORK and VILL) located at a similar latitude, but with about 500 km of baseline which each of them (i.e. between POTS-BORK and LLIV-VILL), are shown in the same plots for comparison. A strong correlation between RMS of the post-fit residuals and the AATR is observed, which is sensitive to several ionospheric features like diurnal variations (large values around noon), Solar Flares (e.g. DoY 301 at noon); both occurring with moderate geomagnetic activity values. Nevertheless, and although the performance is similar for each pair of receivers at a similar latitude (POTS-BORK and LLIV-VILL), a different behaviour is found when comparing the Northern and Southern receivers plots (top and middle plots). Then, the AATR is able to follow the regional behaviour of the ionosphere, as the perturbations are seen at different epochs/days.

Such regional behaviour cannot be represented by planetary indices, like *DST* or *Ap*. For instance, the southern stations like LLIV or VILL, seem to be less linked to the DST that the northern receivers, as BORK and POTS. On the other hand, obviously, the *DST* cannot identify the Solar Flare or other phenomena like those linked to the events around sunset in low or high latitude regions. It is also noticeable the recovering period in the geomagnetic indices (*DST* and *Ap*), which maintains large values during DoY 304 of 2003, while the ionospheric activity suddenly ends at the beginning of this day (see the top and bottom plots).

To extend this comparison with other ionospheric activity indices and other regions, Table 1 shows the correlation coefficient between the post-fit residuals with: AATR, Local Time (LT), *DST*, *Ap* and Solar Flux (*SF*). The table includes six different receivers in Europe and Africa over some tens of days on the last solar cycle, with high ionospheric activity, and all days having DST<*-100 nT*. As it can be seen, the highest correlations are for the AATR index, being typically over 70%. For the geomagnetic indices *DST* and *Ap* the highest correlations are on the northern stations (REYK, ONSA, POTS), while the stations at low latitudes (MAS1, NKLG) are more correlated with the Local Time, which is associated to the after sunset effects, as shown in next sections.

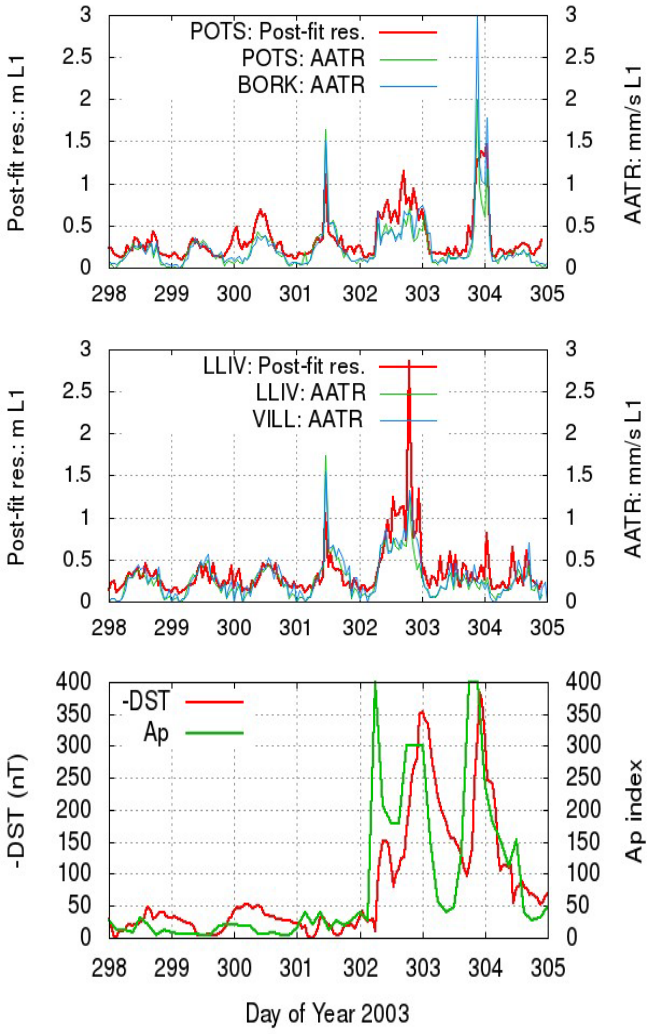

Figure 1. Performance of the AATR index.
Comparison with the RMS of post-fit residuals of an ionospheric model around the Halloween storm for two pairs of stations in the North (BORK and POTS) and in the South (LLIV and VILL) of Europe. The global (geomagnetic) indices DST and Ap are also given in the bottom plot for comparison.

Receiver	Lat (Deg)	Correlation coefficient (×100)				
		AATR	LT	DST	Ap	SF
REYK	64	70	18	-25	30	27
ONSA	57	78	10	-33	35	13
POTS	55	83	11	-29	30	20
CAGL	37	74	26	-13	13	11
MAS1	27	72	47	-7	7	9
NKLG	0	69	52	-24	27	26

Table 1. AATR correlation with other activity indices.

Then, the AATR can be regarded as an indicator of the expected performance of the ionospheric modelling,

without needing to solve the model. It is noteworthy that there is an important difference in the computation load needed to obtain the AATR against the post-fit residuals: while the post-fit residuals require the resolution of an ionospheric model, which can involve up to more than one thousand of parameters, the AATR index can be directly computed from raw GNSS carrier phase measurements (with a reliable cycle-slips detector).

AATR and EGNOS APV1 availability

Taking into account the results of previous section, the feasibility of the AATR index to predict EGNOS APV1 Availability anomalies linked to the ionospheric conditions has been assessed from a detailed analysis of the user domain availability.

Results show that high values of AATR for a given receiver lead to degraded performance in the surrounding areas. A first rough experimental threshold for AATR of *1mm/s of L1* delay was estimated. When AATR is above this value, the performance is clearly degraded as it is shown in Figure 2, where the daily APV1 EGNOS availability and the AATR index are shown for the receiver MAS1 in Canary Islands (ϕ*=27º*, λ*=–14º*). In this figure, the correlation between the large AATR values and the worsening of user availability, over about two year's period, after the EGNOS v2.3.1 upgrade (from May 2012 to August 2014) is presented.

A different comparison between EGNOS availability and the AATR indicator, now for the entire European Civil Aviation Conference (ECAC) region, is given in Figure 3. Its left-hand column shows the EGNOS APV1 availability maps for a nominal day, August 10th 2014, and for three consecutive days of February 27th to March 1st of 2014 having anomalous ionospheric conditions. The associated AATR values for a set of receivers covering a wide range of locations in Europe are shown in the maps in the right hand column. As observed, there is a direct relationship between the worsening in the user domain EGNOS availability and the regional large values of AATR, in line with the results shown in Figure 2.

Finally, the relationship of the AATR with the RMS of the standard deviation of EGNOS corrections (σ_{UIRE}) is depicted in Figure 4 for two different stations TRO1 at ϕ*=69.5º* and SFER in the South of Europe at ϕ*=36.5º*, showing that large uncertainties in the EGNOS ionospheric corrections (σ_{UIRE}) are associated to large AATR values. Notice the correlation in time between the *DST* peak and the AATR and RMS of σ_{UIRE} peaks at the end of Doy 297 for the northern station TRO1, while the behaviour in the southern station SFER is not linked to the DST.

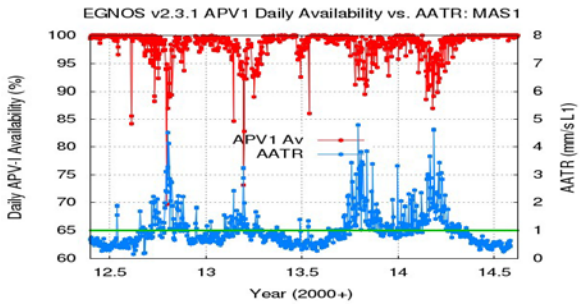

Figure 2. AATR and EGNOS APV1 availability. Relationship between the daily EGNOS APV1 availability (in red colour) and the daily maximum values of AATR (in blue colour). This result corresponds to a Fault-free receiver in Canary Islands (MAS1) from May 25th 2012 to August 15th 2014 (after the EGNOS v2.3.1 upgrade). The horizontal green line indicates an experimental threshold for AATR of *1 mm/s* of L1 delay.

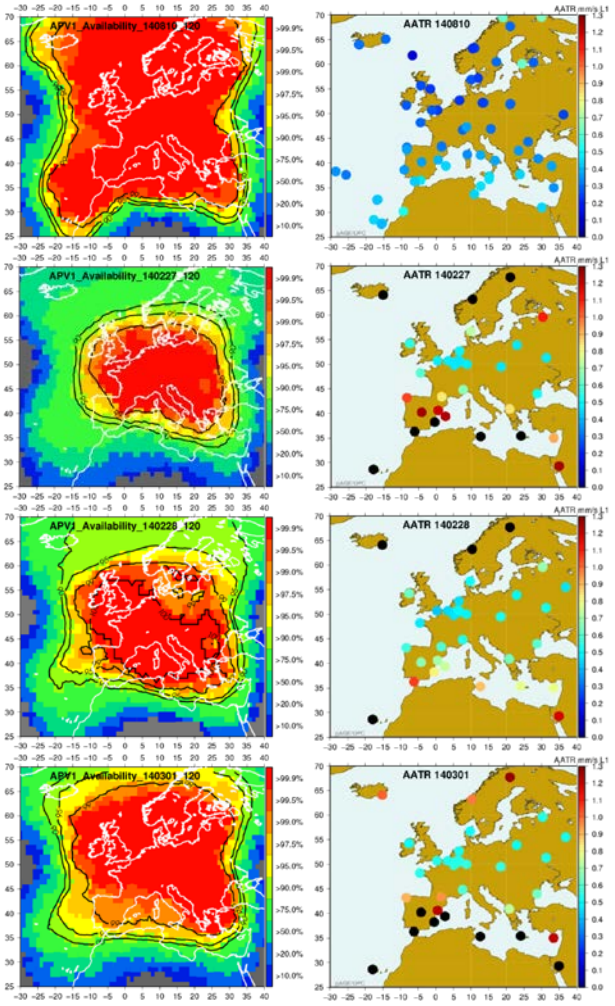

Figure 3. EGNOS APV1 availability (left) and AATR (right) maps under nominal and degraded ionospheric conditions. The first row map corresponds to a nominal day (August 10th 2014). The next maps correspond to three consecutive days, from February 27th (Doy 058) to March 1st (Doy 60) of 2014. A clear relationship between EGNOS availability and AATR values is shown in the maps. The colour bar for the AATR map is in mm/s of L1 delay, saturating at *1.3mm/s*. Over this threshold, the values are depicted in black colour.

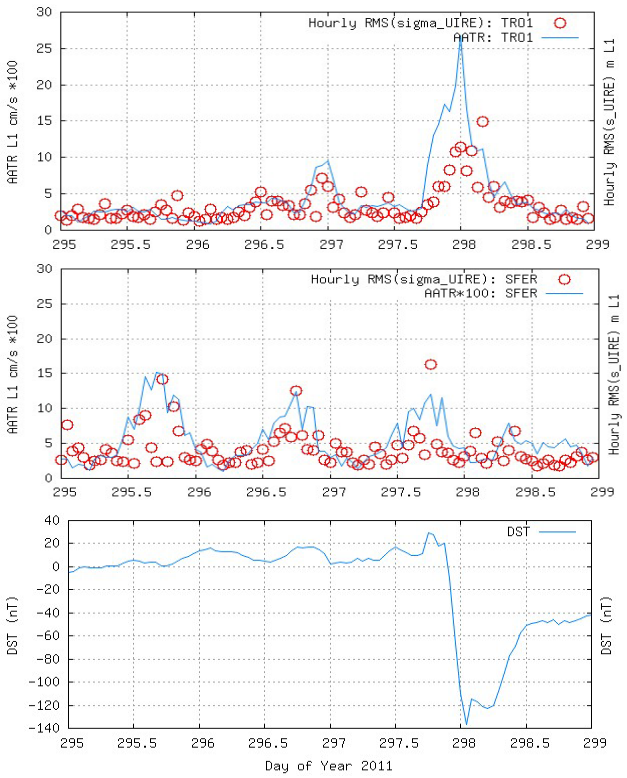

Figure 4. AATR and RMS of hurly σ_{UIRE}.
The top plot is for the receiver TRO1 in the North of Europe and the middle plot is for the receiver SFER in the South of Europe. The time interval ranges from DoY 295 to 299 of 2011. The bottom plot shows the DST index.

AATR STATISTICAL VALUES OVER THE LAST SOLAR CYCLE

In order to consolidate the AATR as an indicator of ionospheric disturbed periods, it has been computed for a set of 140 IGS receivers during more than a Solar Cycle (from 2002 to the end of 2013, involving 4351 days in total). Obviously, not all the receivers were available during every day of this period of time, but at least 100 receivers were used for any given day. The geographical distribution of receivers involved in the AATR computations is depicted in Figure 7.

The analysis of the AATR values along a Solar Cycle has shown that this index follows similar temporal dependencies than the Total Electron Content (TEC), as found in [7], that is:

- The AATR values are related with the Solar Flux, achieving the largest values during the years of Solar Cycle maximum. For instance, the daily mean AATR values for a set of 8 receivers with quite different coordinates are depicted in Figure 5 for the entire period analysed. As it can be seen, in all these receivers, the AATR value is modulated by the Solar Cycle.

	LON	LAT	MODIP
GOLD	-116.9	35.2	49.6
HARB	27.7	-25.7	-48.3
HERS	0.3	50.7	55.3
INVK	-133.5	68.2	66.8
KOUR	-52.8	5.2	19.1
MCM4	166.7	-77.8	-72.0
NKLG	9.7	0.4	-23.9
TRO1	18.9	69.5	66.5

Table 2. Coordinates of receivers used in the study of temporal dependences.

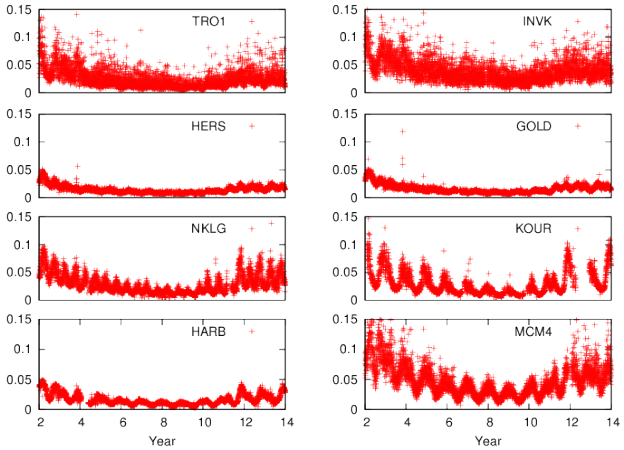

Figure 5. Daily mean AATR (cm/s L1) value along the last Solar Cycle, for the receivers of Table 2.

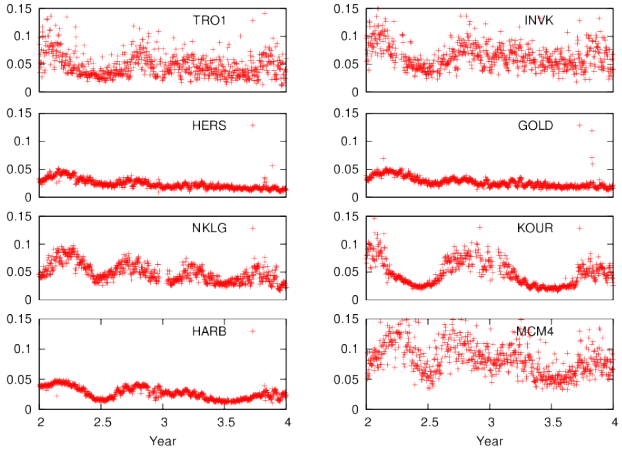

Figure 6. Zoom of previous figure over period 2002-2004.

The receiver coordinates are given in Table 2, which includes also the MODIP Angle.

The receiver *MODIP* angle is defined as:

$$MODIP = \frac{DIP}{\sqrt{\cos\phi}} \qquad (5)$$

where DIP is the so called geomagnetic DIP angle, that is, the angle between the downwards radial component and the horizontal component, and ϕ is the geographic latitude of the receiver. In this study we have used the IGRF-2003 geomagnetic model [9].

- Along the year, the AATR is higher close to the equinoxes (around days of year 100 and 300), being the values of the December solstice typically higher than the June solstice ones. This can be seen in Figure 6 which is a zoom of Figure 5 for the period 2002-2004. Here the most relevant feature is the different periodicity between the receiver KOUR (in South America) and the rest of receivers. Indeed the daily mean AATR value in KOUR (and also in the other South American receivers) has a clearly annual periodicity with the maximum at the December Solstice, while the other receivers (including the low latitude ones, as NKLG) have a semi-annual periodicity with the maximum values around the equinoxes.

- Finally, as the TEC, the AATR follows, in general, the daily variation associated to the ionisation process. But, as we will see later this is not true in all the cases.

As commented in the introduction one of the main goals of this study was to identify ionospheric worst-case scenarios. In this sense, and thanks to the large historical data set analysed, we have been able to identify the period with largest ionospheric activity. The 20 receivers, among the 140 above mentioned, having the maximum values of AATR during the last solar cycle (i.e. from 2002 to 2013) are shown in Table 3, column 7th in bold. As it can be seen, the largest AATR values over these last 12 years occurred during the ionospheric super-storms on 2003 (days 302-304 and 324). These largest values were experienced not only on high latitude receivers but also in mid-latitude (GODE, USNO, AMC2, DRAO) having similar values during such disturbed periods. It should be noted that these maximum values are actually rare events, in the tail of the probability distribution, being up to one order of magnitude larger than the 99,7th percentile (also depicted in Table 3). Low latitude receivers (KOUR, BRAZ) also appear in Table 3, but in spite of having also large values during ionospheric super-storms, these events are also linked to local time and to a seasonal behaviour, as we will see later. For instance, the station KOUR reached the maximum value on day 355 of year 2002, not directly related with a storm (DST> -75 nT during this day).

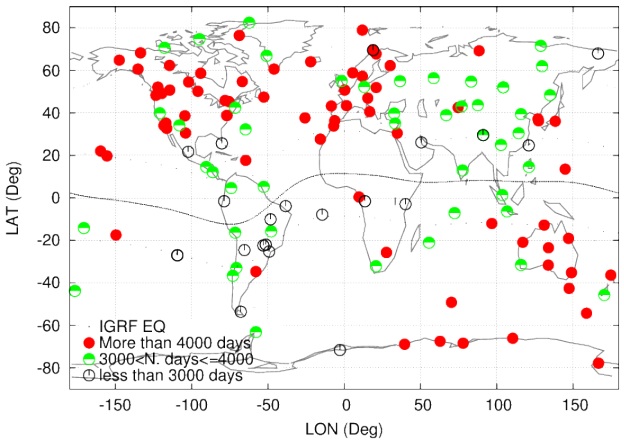

Figure 7. Geographical distribution of receivers. Geographical distribution of processed receivers, with indication of number of days processed. Red circles are for more than 4000 days. Green circles indicate the number of days between 3000 and 4000, and black circles, less than 3000 days.

RCV	LON	LAT	MODIP	# values	99.7th	100th	day
mcm4	166.7	-77.8	-72.0	100821	0.28	**1.38**	2003303
yell	-114.5	62.3	64.3	100895	0.23	**1.27**	2003303
reso	-94.9	74.6	71.5	93482	0.15	**1.22**	2003303
gode	-76.8	38.8	53.0	98844	0.06	**1.11**	2003324
usno	-77.1	38.7	53.0	93592	0.08	**1.05**	2003324
flin	-102.0	54.5	60.8	100035	0.20	**1.04**	2003303
holm	-117.8	70.6	68.8	94342	0.22	**1.04**	2003303
kour	-52.8	5.2	19.1	85740	0.29	**1.00**	2002355
cas1	110.5	-66.1	-66.1	98208	0.31	**0.99**	2002278
prds	-114.3	50.7	58.3	95826	0.09	**0.97**	2003303
chur	-94.1	58.6	63.0	95246	0.25	**0.91**	2003303
will	-122.2	52.1	58.5	96181	0.08	**0.90**	2003303
amc2	-104.5	38.6	52.6	101858	0.08	**0.85**	2003303
drao	-119.6	49.1	57.1	102833	0.08	**0.85**	2003302
lpgs	-57.9	-34.7	-36.3	94453	0.12	**0.83**	2003303
thu3	-68.8	76.4	72.1	98162	0.22	**0.82**	2003303
whit	-135.2	60.6	62.3	94944	0.18	**0.80**	2003303
braz	-47.9	-15.8	-20.4	88066	0.31	**0.80**	2002344
maw1	62.9	-67.5	-63.0	91439	0.20	**0.80**	2002134
tro1	18.9	69.5	66.5	102261	0.18	**0.79**	2003324

Table 3. the 20th largest values of AATR (in cm/s L1) and its 97th percentile.

In Table 3, the MODIP is also included, which is found a more suitable parameter than the latitude to classify the ionospheric activity regions as it is shown later on.

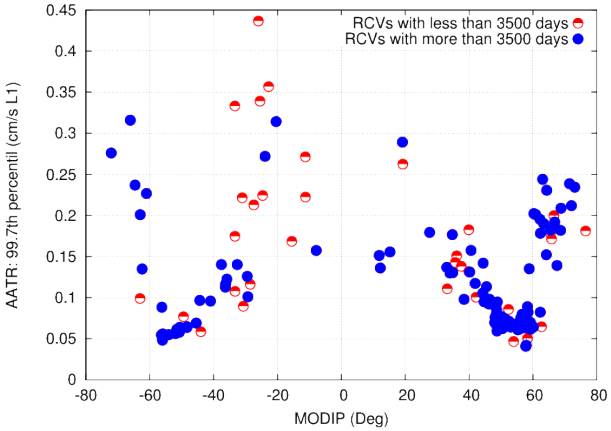

Figure 8. The 99.7th percentile of AATR (cm/s L1) as a function of MODIP for 2002 to 2013 period.

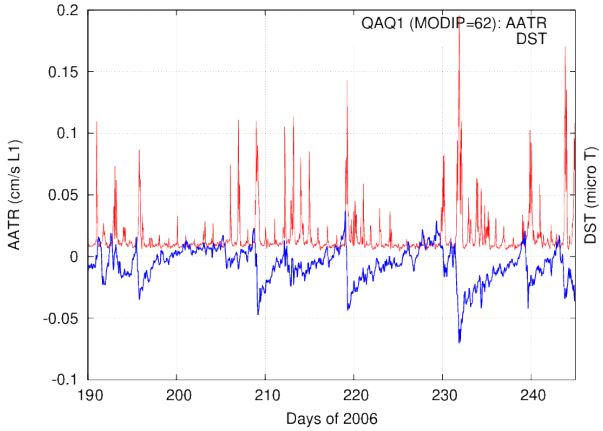

Figure 9. Relationship between AATR and the DST for a high latitude receiver (QAQ1, ϕ=61º, MODIP=62º).

A more statistically significant parameter than the maximum value is the 99.7th percentile, which is also given in Table 3 for the receivers with largest AATR. This percentile is depicted in Figure 8 for all the receivers involved in the study as a function of their MODIP. In this plot it is observed that the largest values occur in both high (|MODIP|>60º) and low latitude (|MODIP|<39º) receivers. These results confirm the ones obtained with a lower set of receivers (see those in Table 1) and agree with other studies devoted to scintillation (see for instance [8] and references therein). This is because disturbances associated to the observation of ionospheric scintillation are also often related to the increase of AATR values in polar and equatorial regions. But large values of AATR are also experienced without scintillation. Indeed, the AATR is thought to detect ionospheric irregularities in general and at regional scale, and thence, can reach large AATR values even in absence of scintillation. Notice that the AATR is computed from all in view measurements, and therefore, it is associated to the receiver in a given region, and not to a single satellite-receiver arc. It is noteworthy that, in spite of low and high latitude receivers experiencing the largest AATR values, these events seem to be linked to different phenomena:

1) In high latitude receivers, the large values of AATR are related to space weather events (solar-geomagnetic interactions), showing a high correlation between the AATR and *DST*. Typical examples are shown in Figure **9** and Figure 4.

2) In the low latitude receivers, the highest values of AATR occur around the sunset hours (similarly to ionospheric scintillation in this region), being more noticeable on the years around the Solar Cycle maximum and close to the equinoxes. However, as shown in Figure 10 its magnitude and climatology seems to depend on the receiver geographical longitude and the epoch of the year.

To depict this dependency of AATR with the longitude, the hourly AATR values are separated in two groups Figure 11: i) Those occurring around the Solar Terminator (ST), in blue, and ii) those measured during any other epoch, in red. This is done for four low latitude receivers, two of them in South America (BOGT and BRAZ), a third one in Africa (NKLG) and the last one in the South East of Asia (NTUS). As it can be seen, while the temporal dependency of the AATR values over epochs far from the ST (red points) is quite similar for the four receivers (presenting a semi-annual periodicity), the AATR values around the ST (blue points) are quite different for the low latitude receivers: annual for the South-American region and semi-annual for the others. In fact, such behaviour is the origin of the different periodicities seen in Figure 6.

3) Finally, mid-latitude receivers do not experience large AATR values, except under super-storms as shown in Table 3.

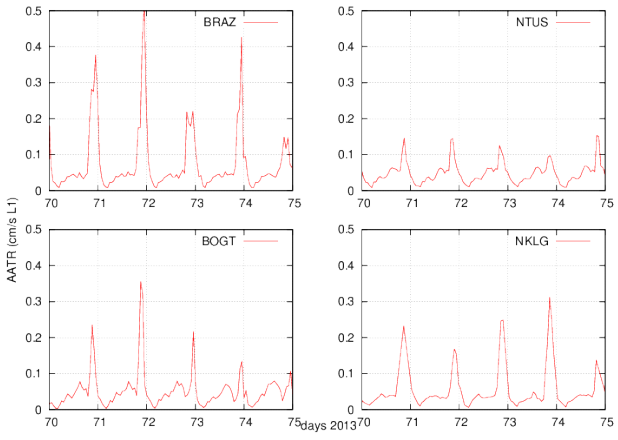

Figure 10. Hourly AATR values during five days of 2013. The four plots correspond to low latitude receivers in South America, left side panels (BRAZ, BOGT), in South-East of Asia at the top right panel (NTUS), and in Africa at the bottom right panel (NKLG). The units are cm/s of L1 delay.

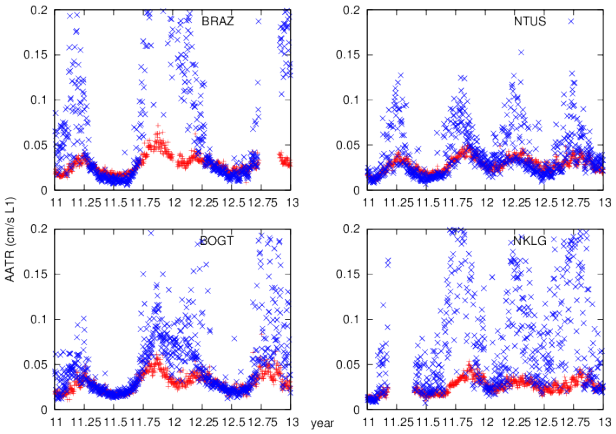

Figure 11. AATR on sunset and non-sunset events.
AATR associated to around sunset events (18 < LT < 23) are shown in blue. The non-sunset events (LT<18 or LT>23) are shown in red. The four plots correspond to low latitude receivers in South America, left side panels (BRAZ, BOGT), in South-East of Asia at the top right panel (NTUS), and in Africa at the bottom right panel (NKLG).

IONOSPHERIC ACTIVITY REGIONS

After the exhaustive analysis and the examples showing the behaviour in different ionospheric regions, we are now able to characterise the activity regions. Indeed, in the previous section we have found that in mid latitude regions the AATR reaches high values only during ionospheric super storms. In low latitude receivers the largest AATR values are achieved around the ST, while the AATR is quite moderate during other times. Finally in high latitude regions, the AATR is affected by geomagnetic disturbances not linked to local time.

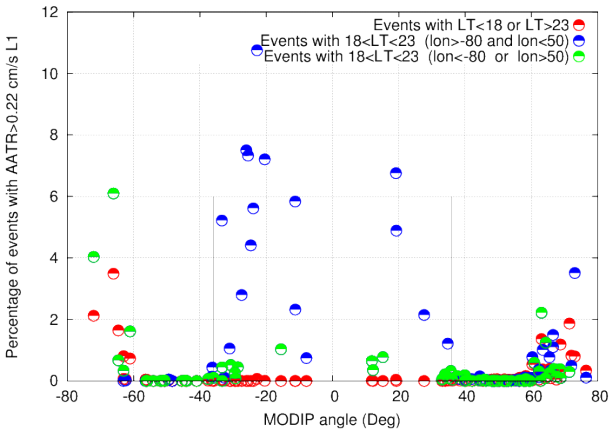

Figure 12. Percentage of events with AATR over 0.22 cm/s L1, as a function of the receiver MODIP.
The non-sunset events (LT<18 or LT>23) are shown by red symbols. The sunset events (18 < LT < 23) for receivers around the Atlantic South anomaly are depicted as blue circles. The sunset events far from the Atlantic South anomaly (Lon > 50 and Lon< -80) are indicated by green circles. The vertical lines in black indicate the separation between the different regions in MODIP.

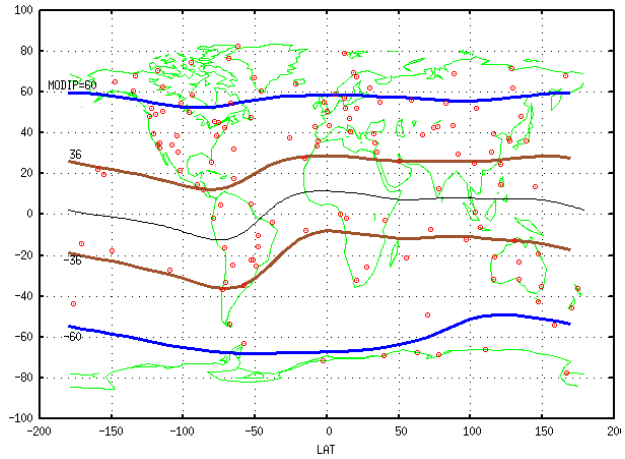

Figure 13. Ionospheric activity regions associated to the MODIP bounds of Figure 12.

Following the previous considerations, the AATR index is used in this section to define different ionospheric activity regions as a function of MODIP. A devoted study over the years with high solar flux values (2002-2003, 2012-2013) have lead to a criteria based on the probability (percentage of cases) of having an AATR>0.22 L1 cm/s to define such regions. This threshold has been selected according to the results of Figure 8, but other values provide similar outcomes. Figure 12 shows these percentages, with the events classified by around sunset and non-sunset. From this figure it follows the next classification:

- $|MODIP| > 60^o$

  In this region, a significant percentage of events with AATR>0.22 L1 cm/s are found, linked to both sunset events (green circles) and non-sunset events (red circles).

- $36^o < |MODIP| < 60^o$

  This is a very quiet region, without experiencing events with AATR > 0.22 L1 cm/s.

- $|MODIP| < 36^o$

  This region has the larger percentage of events with AATR>0.22 L1 cm/s, which are only linked to around sunset events, specifically for receivers around the Atlantic South anomaly (blue circles in Figure 12). For other longitudes, the AATR values are more moderated (green circles).

A map with the different regions associated to the previous MODIP bounds is given in Figure 13.

CONCLUSIONS

In this work we have defined a new ionospheric activity indicator which enables to detect regional ionospheric disturbances and can be easily computed from the GNSS data. For a given receiver, this indicator is based on the hourly RMS of the Along Arc TEC Rate (AATR).

The AATR is considered as an indicator of the expected performance of the ionospheric modelling. In this way, we have evaluated its performance to predict the degradation of the ionospheric modelling during disturbed conditions. This evaluation has been done with the help of a precise ionospheric model, analysing its performance under different ionospheric conditions and validating the results with the AATR indicator. Results show a high correlation between the AATR values and the post-fit residuals of the ionospheric model (correlation coefficient larger than 0.7 in all latitudes, well above the correlation coefficient values obtained with other indicators such as *DST* or *Ap* indices).

The AATR index has been used to identify the conditions where a degradation in the user performance of the SBAS systems in general, and in EGNOS in particular, is expected. In this way, the daily APV1 EGNOS availability has been analyzed for more than two years period after the EGNOS v2.3.1 upgrade (from May 25th 2012 to August 15th 2014). Results show that high values of this index for a given station leads to worse performances in the EGNOS APV1 availability in the surrounding area due to the ionospheric conditions. Indeed, we have shown that it is possible to predict the EGNOS user availability over the ECAC region from a small set of receivers.

Finally, a study on the AATR performance has been done during more than one Solar Cycle, from 2002 to the end of 2013, with 4351 days in total, and involving 140 IGS receivers distributed worldwide. Results show a clear regional and temporal dependence, at different scales. For instance, solar cycle periodicities, and annual and semi-annual dependences can be found depending on the region. In particular, we have shown that, three regions can be defined attending to the statistical analysis of AATR values:

- High latitude receivers exhibit large AATR values related with high (or even moderate) geomagnetic activity.
- The lower AATR values are found in mid latitude regions, being latitude dependent (the AATR increase towards the equator), but always with moderate values. However, during geomagnetic super-storms, the AATR in mid-high latitude receivers can reach values at the level of the high latitude ones.
- Finally, in low latitude regions the largest AATR values are mainly linked to the around sunset events. They have clear seasonal dependences, as well as with the solar cycle. Moreover, a longitude dependent behaviour is also found.

The AATR index has been chosen as the metric to characterise the ionosphere operational conditions in the frame of EGNOS activities. This indicator has been also proposed for joint analysis in the International SBAS-Ionosphere Working Group.

ACKNOWLEDGMENTS

This work has been carried out under the ICASES and ICASES2 projects from ESA under EC delegation agreement. We also would like to thank to the Spanish Ministry of Science and Innovation project CTM2010-21312-C03-02 and the GNAVIS project from EC-FP7 Grant Nr. 287203.

REFERENCES

[1] S. Datta-Barua, Ionospheric Threats to the Integrity of Airborne GPS users. PhD thesis. Stanford, CA, USA: Stanford University, 2008.

[2] S. Datta-Barua, T. Walter, E. Altshuler, J. Blanch, and P. Enge, “Dst as an Indicator of Potential Threats to WAAS Integrity and Availability,” in Proceedings of ION GPS 2005, Long Beach, CA, USA, Sep. 2005, pp. 2365–2373.

[3] C. Mayer, B. Belabbas, N. Jakowski, M. Meurer, and W. Dunke, “Iono sphere Threat Space Model Assessment for GBAS,” Proceedings of the 22 International Technical Meeting of the Satellite Division of the Institute of Navigation, Savannah, GA, 2009, pp 1091-1099

[4] N. Jakowsky, C. Borries, and V. Wilken, “Introducing a disturbance ionosphere index.” Radio Science, vol. **47**, 2012.

[5] S. Schluter, R. Prieto-Cerdeira, R. Orús Pérez, J. Lam, J. Juan, J. Sanz, “Characterization and Modelling of the ionosphere for EGNOS Development Qualification”, European Navigation Conference (ENC2013), Vienna 2013.

[6] M. Juan, M. Hernández-Pajares, J. Sanz, P. Ramos-Bosch, A. Aragon-Angel, R. Orus, W. Ochieng, S. Feng, P. Coutinho, J. Samson, and M. Tossaint, “Enhanced Precise Point Positioning for GNSS Users.” IEEE Transactions on Geoscience and Remote Sensing 10.1109/TGRS.2012.2189888, vol. **50**, No 10, pp. 4213-4222, 2012.

[7] M. Hernández-Pajares, J. M. Juan, J. Sanz, R. Orus, A. Garcia-Rigo, J. Feltens, A. Komjathy, S. Schaer, "The IGS VTEC maps: a reliable source of ionospheric information since 1998", Journal of Geodesy, Vol. 83, pp. 263-272, 2009 (DOI 10.1007/s00190-008-0266-1).

[8] Y. Béniguel et al. “Ionospheric scintillation, monitoring and modelling”. Annals of Geophysics, Vol. 52, N. 3/4, June/August 2009.
[9] Tsyganenko, N.A. (2003). A set of FORTRAN subroutines for computations of the geomagnetic field in the Earth’s magnetosphere (Geopack), Univ. Space Res. Assoc., Columbia, Md.